Available online at www.sciencedirect.com
SCIENCE DIRECT®
Journal of Crystal Growth 277 (2005) 13–20
JOURNAL OF CRYSTAL GROWTH
www.elsevier.com/locate/jcrysgro

>100% output differential efficiency 1.55-μm VCSELs using submonolayer superlattices digital-alloy multiple-active-regions grown by MBE on InP

C.S. Wang[a,*], R. Koda[a], A.S. Huntington[b,c], A.C. Gossard[b], L.A. Coldren[a,b]

[a]*Department of Electrical and Computer Engineering, University of California, Santa Barbara, CA 93106, USA*
[b]*Department of Materials, University of California, Santa Barbara, CA 93106, USA*
[c]*Voxtel, Inc., Beaverton, OR 97005, USA*

Received 30 October 2004; accepted 23 December 2004
Communicated by D.W. Shaw
Available online 1 February 2005

Abstract

High-quality InAlGaAs digital-alloy active regions using submonolayer superlattices were developed and employed in a 3-stage bipolar cascade multiple-active-region vertical cavity surface emitting laser (VCSEL) design. The photoluminescence intensity and linewidth of these active regions were optimized by varying the substrate temperature and digitization period. These active regions exhibit considerable improvement over previously developed digital-alloy active regions and are comparable to analog-alloy active regions. Multiple-active-region VCSELs, grown all-epitaxially by MBE on InP, demonstrate greater than 100% output differential efficiency at 1.55-μm emission. A record high 104% output differential efficiency was achieved for a 3-stage long-wavelength VCSEL.

PACS: 42.55.Px; 78.66.−w; 81.15.Hi

Keywords: A1. Photoluminescence; A3. Molecular beam epitaxy; A3. Quantum wells; B3. Laser diodes; B3. Vertical cavity lasers

1. Introduction

Multiple-active-region (MAR) vertical cavity surface emitting lasers (VCSELs) are a novel approach to develop high output power VCSELs [1,2]. MAR can allow for differential efficiencies greater than unity, which could be used to make low-noise, transparent optical links, or even links with gain [3,4]. In this approach, active region stages are epitaxially stacked in series with Esaki tunnel junctions that effectively 'recycle' current to each stage of the active region, as illustrated in Fig. 1. Electrons injected into an active region can

*Corresponding author. ECE Department, UC Santa Barbara, CA 93117, USA. Tel.: +1 805 893 7065; fax: +1 805 893 4500.
E-mail address: cswang@engineering.ucsb.edu (C.S. Wang).

0022-0248/$ - see front matter © 2005 Elsevier B.V. All rights reserved.
doi:10.1016/j.jcrysgro.2004.12.139

recombine to emit a photon, but can then tunnel into subsequent active region stages. This cascading of N_a active regions with tunnel junctions can theoretically lead to N_a photons for every one electron. Furthermore, the threshold current scales sublinearly with $1/N_a$. Detailed analysis of the scaling properties of MAR devices can be found in Refs. [1,2,5]. To realize high performance MAR VCSELs, high-quality active regions must be developed. This is necessary in order to achieve the high gain necessary for high output efficiency. Previously at 1.55-μm emission, 94% output differential efficiency was shown grown with analog-alloy active regions [2]. In the work presented in this paper, high-quality digital-alloy active regions (DAAR) using submonolayer superlattices (SMS) were developed and implemented into a 3-stage MAR VCSEL with greater than 100% differential efficiency.

The structures were grown by molecular beam epitaxy (MBE), a popular method for all-epitaxial VCSELs due to its precise control over layer thicknesses. The technique of digitally grown alloys also alleviates the need for multiple group III sources or changes in cell temperature during growth. This technique has been successfully used in a wide variety of structures, such as light emitters [6], graded structures [7,8], and distributed Bragg reflectors (DBRs) [9], to name a few. Digital alloys can also be applied to active regions to utilize the control over precise composition and strain. In the long-wavelength regime, InAlGaAs-based quantum wells and barriers can be easily tailored to span across the 1.31–1.55 μm range. Furthermore, InAlGaAs-based active regions are preferred for their high temperature performance [10]. Previous work on long-wavelength DAAR with short period superlattices and SMS has shown improved uniformity and compositional accuracy using a variety of binary and ternary superlattice combinations, such as binary—binary SMS [11,12], lattice-matched ternary (LMT)—strained ternary superlattices [13], and binary—LMT SMS [14,15]. These techniques have demonstrated edge emitting lasers with low threshold current densities. In this work, we use a binary—LMT SMS technique similar to Reddy et. al. due to the relative ease of implementation since the growth depends only on two parameters: ternary lattice matching condition and their growth rates [15]. However, the dependence on the digitization period and growth conditions has not been well studied and documented.

In this paper, we first investigate the growth parameters to optimize the growth of high-quality DAAR using SMS. These active regions, targeted to 1.55-μm, are then applied to an all-epitaxially grown 3-stage MAR VCSEL. The devices demonstrate greater than 100% output differential quantum efficiency, the highest ever reported for a 3stage long-wavelength VCSEL, with low threshold voltages and current densities.

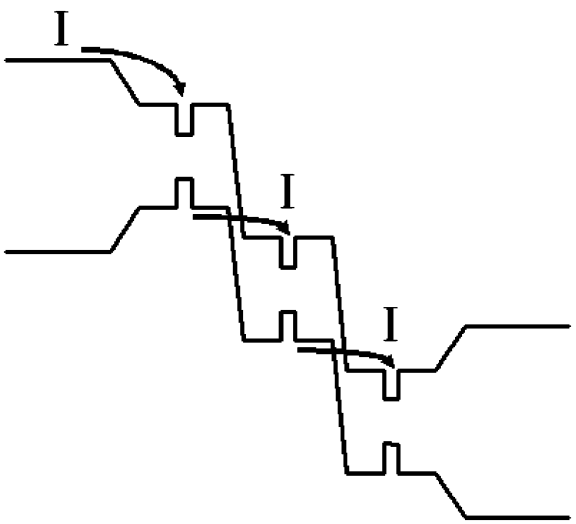

Fig. 1. Schematic illustration of a MAR VCSEL operation.

2. Experimental procedure

The experimental work reported on in this paper first investigates the growth of high quality DAAR using SMS at 1.55-μm. These were optimized for photoluminescence (PL) intensity and linewidth full width half max (FWHM). Then, the structure and growth conditions for a MAR VCSEL using the optimized DAAR is described. Finally, broad area VCSELs were fabricated and tested.

The growths for this work were performed in an ultra-high vacuum Varian Gen II solid-source

MBE system. A valved arsenic cell was the only group V source present for our machine, thus preventing any growth of InP for buffer or heat-spreading layers in the VCSEL.

2.1. Digital-alloy active region optimization

The DAAR were optimized by varying the SMS periodicity, Λ, and the active region substrate temperature, as measured by an optical pyrometer. The substrate temperatures quoted in this work were measured while idling with arsenic overpressure only. (With the group III cells open, the substrate temperature reads 10–20 °C hotter.) Fig. 2 shows the structure grown to evaluate the DAAR. The structure consists of a 200 nm $In_{0.52}Al_{0.48}As$ buffer followed by a 500 nm $In_{0.52}Al_{0.34}Ga_{0.14}As$. This buffer layer, like all other InAlGaAs layers grown in this work, was grown digitally using appropriate amounts of $(In_{0.53}Ga_{0.47}As)_{1-x}(In_{0.52}Al_{0.48}As)_x$. Sandwiched in between $In_{0.52}Al_{0.29}Ga_{0.19}As$ is the active region, nominally designed for 1530 nm emission. The active regions consist of five 70 Å thick, compressively strained $In_{0.70}Al_{0.07}Ga_{0.22}As$ quantum wells with six 50 Å thick, tensile strained $In_{0.44}Al_{0.12}Ga_{0.44}As$ barriers. A matrix of growths was performed varying the active region substrate temperature from 500 °C to 590 °C with a SMS periodicity of 3.5 Å. At active region substrate temperatures of 530 °C and 560 °C, the SMS periodicity was varied from 3.5 Å up to 17 Å. Table 1 lists the digitization schemes used for the SMS. Finally, all buffer layers were grown at 500 °C with an arsenic overpressure of 8×10^{-6} Torr, equivalent to a V/III ratio of 18, as optimized in a separate study for smoothest epitaxial films [16].

The quality of the DAAR was evaluated by room temperature PL for intensity and FWHM, and atomic force microscopy (AFM) for surface roughness. Fig. 3 shows PL curves for a few DAAR grown at varying substrate temperatures. As the active region is grown hotter, the PL wavelength blue shifts due to indium desorption. Figs. 4 and 5 plot the peak PL intensity and FWHM, respectively, as a function of substrate temperature for the entire matrix set. First, for short SMS periodicities ($\Lambda < 10$ Å), the most noticeable trend is that the peak PL intensity is maximized for DAAR grown between 520 °C and 530 °C. Likewise, the FWHM minimizes to around 35 meV at those temperatures. At higher temperatures, the PL begins to degrade and broaden; this corresponded to an increase in material roughness as a result of deviating from the window of smooth growth. However, the dependence on SMS periodicity is less obvious. At the cooler substrate temperatures of 530 °C, the peak PL intensity and FWHM does not degrade until a SMS periodicity of 17 Å. However, for DAAR grown at 560 °C, a SMS periodicity of 17 Å does not significantly differ than those of shorter periodicities. This is due to inhomogeneous material at the colder substrate temperatures. At longer SMS periodicities grown colder, the epitaxial film forms

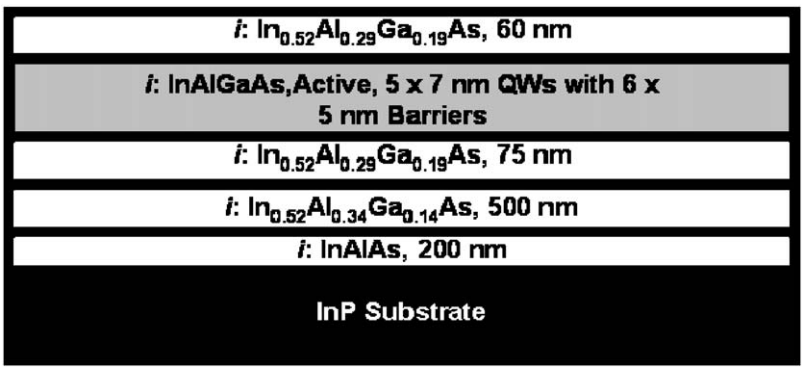

Fig. 2. Epilayer structure used in DAAR optimization study.

Table 1
SMS periodicity, thickness, and layer sequence used in the DAAR

	Thickness (Å)	Target SMS period, Λ (Å)	Actual SMS period, Λ (Å)	Repetitions	SMS layer sequence—thickness (Å)
Barrier	50	3.5	3.572	14	
		5	5.008	10	InGaAs–Λ/3.4182
		7	7.144	7	AlInAs–Λ/4.0
		10	10.0016	6	InGaAs–Λ/3.4182
		17	16.6667	3	GaAs–Λ/6.0645
Quantum well	70	3.5	3.503	20	InGaAs–Λ/4.1802
		5	5.3892	13	InAs–Λ/5.4734
		7	7.0057	10	AlInAs–Λ/6.404
		10	10.0054	7	InGaAs–Λ/4.1802
		17	17.5095	4	InAs–Λ/5.4734

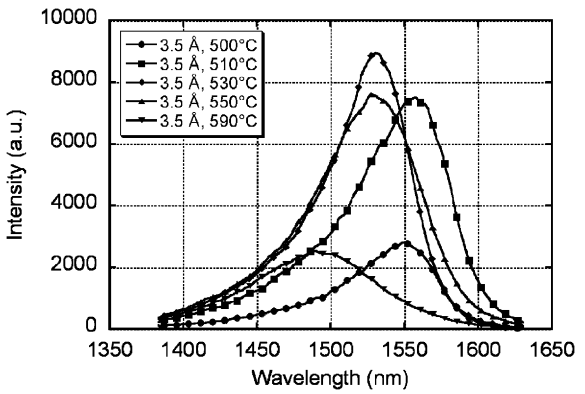

Fig. 3. PL of DAAR grown with a SMS periodicity of $\Lambda = 3.5$ Å at varying substrate temperatures.

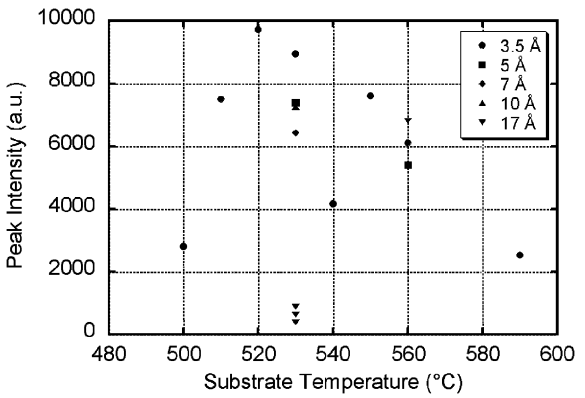

Fig. 4. PL peak intensity of DAAR grown with varying SMS periodicity, Λ, at varying substrate temperatures.

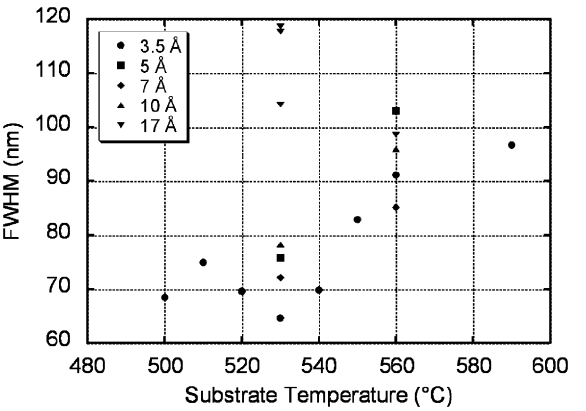

Fig. 5. PL full width half maximum of DAAR grown with varying SMS periodicity, Λ, at varying substrate temperatures.

spontaneous lateral composition modulations due to strain and islanding in the material, leading to poor superlattice [17]. This is confirmed by high surface roughness for these samples, which are in excess of 10 Å rms. However, when grown under hotter conditions, the epitaxial film is given more energy to migrate and form more homogeneous films.

From this experiment, an acceptable growth window for DAAR has been identified. Low SMS periodicities are desirable with substrate temperatures between 520 °C and 530 °C. Of course the periodicity of the SMS is ultimately limited by the speed of the shutter operation. Lastly, bright room temperature PL was observed with FWHM as low

as 33 meV, better than previous DAAR [14,18], and comparable to analog-alloy based active regions [19,20].

2.2. MAR VCSEL growth and fabrication

The technology used for this MAR VCSEL include the use of InAlGaAs/InAlAs DBRs and InAlGaAs active regions, lattice-matched to InP. This material system has the inherent drawback of low thermal impedance and low refractive index contrasts. However, this can be alleviated with the inclusion of InP as a heat spreading layer and well calibrated growth. Nevertheless, this technology was chosen for its capability to be grown all-epitaxially. The epilayers for the bottom emitting MAR VCSEL structure are shown in Fig. 6. The bottom and top DBRs are composed of 35.5 and 45.5 periods, respectively, of $In_{0.53}Al_{0.1}Ga_{0.38}As/In_{0.52}Al_{0.48}As$, and are compositionally graded at the interfaces. This results in reflectivities of 98.9% and 99.9% for the bottom and top DBRs, respectively. The doping in the DBRs is varied n-type from $2.5 \times 10^{18}\,cm^{-3}$ farther away from the active region down to $1 \times 10^{18}\,cm^{-3}$ nearer to the active region. The undoped separate confinement heterostructure (SCH) cladding layers are composed of $In_{0.52}Al_{0.29}Ga_{0.19}As$. The tunnel junctions are 350 Å thick similarly composed of $In_{0.52}Al_{0.29}Ga_{0.19}As$, with 220 Å for the n++-side and 130 Å for the p++-side. Silicon is used as the n-dopant and carbon for the p-dopant. The same active region composition as used in the DAAR optimization experiment was used for the VCSEL.

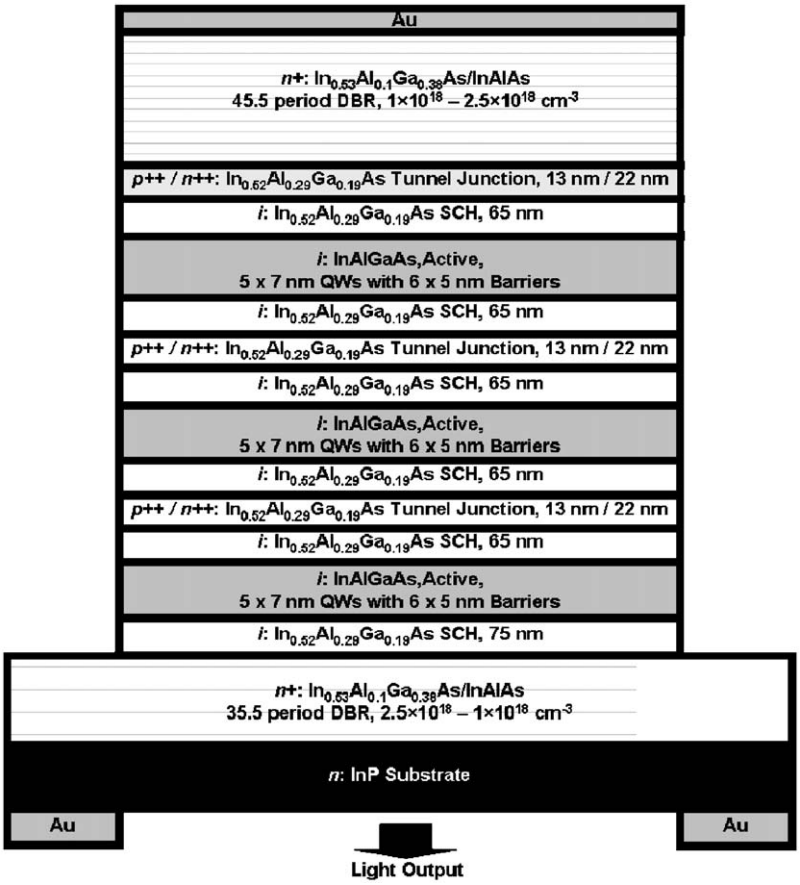

Fig. 6. Epilayer structure for the 3-stage MAR VCSEL.

The epilayers were grown on a sulfur doped n-type InP (1 0 0) wafer. Growth was preceded first with oxide desorption. The substrate was heated under very slight arsenic pressure (5×10^{-7} Torr) to 520 °C, upon which growth commenced while the substrate cooled to its growth temperature of 500 °C. An arsenic overpressure of 8×10^{-6} Torr was used during growth, facilitating a growth rate of 1 μm per hour. During growth of the n-side of the tunnel junction, the substrate temperature was reduced to 450 °C and the arsenic overpressure was increased to 2×10^{-5} Torr. This was found to increase the silicon doping concentration. The active region was grown at 530 °C with a 3.5 Å SMS digitization period.

The measured and designed reflectivity spectra of the MAR VCSEL is shown in Fig. 7, with the measured optical cavity at 1551 nm sandwiched between an approximately 100 nm wide stopband. The decreased reflectivity dip at around 1505 nm is due to absorption from the $In_{0.53}Ga_{0.47}As$ contact layer and the dip at 1580 nm is due to slight misalignment of the top and bottom DBRs. Next, the surface roughness between defects measured by AFM was 2.23 Å, indicating smooth superlattice growth throughout the epilayers. The low surface roughness is necessary for the high-quality active regions and low optical scattering in the DBRs [21].

Broad area pillars ranging from 25- to 100-μm in diameter were fabricated. First, the top mirror contact metal (Ti/Pt/Au) immediately followed by a dielectric etch mask (SrF_2) was deposited and lifted off to form the pillars. Next, a dry etch was used to etch straight sidewall pillars through the active region. After removing the etch mask, backside metal (Ni/AuGe/Ni/Au) was deposited onto the substrate, and the contacts were annealed. Lastly, a MgO anti-reflection (AR) coating was deposited on the substrate output interface.

3. Results and discussion

The devices were tested under room temperature pulsed operation with 500 ns pulses at a repetition rate of 1 kHz. The devices exhibited excellent voltage and light output power characteristics, and all lased multimode at around 1537 nm wavelength. Average output differential efficiencies were 70%, 90%, and 95%, for 25, 50, and 100-μm diameter devices, respectively, as shown in Fig. 8. Fig. 9 shows the best LIV performance at each device size. 104% differential efficiency was achieved for the 100-μm diameter device. Absorption from the 500-μm thick n-doped substrate was not taken into account, leading to approximately 15% more output power [2]. This would result in a record high 119% differential quantum efficiency for a 3-stage long-wavelength VCSEL. The decrease in output efficiency for the 25-μm diameter

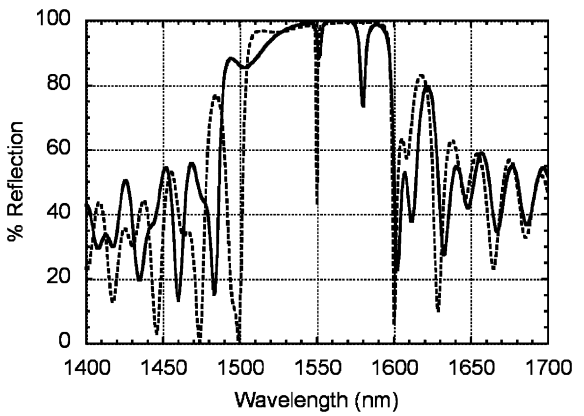

Fig. 7. Measured (solid) and simulated (dashed) reflectivity spectrum of the MAR VCSEL.

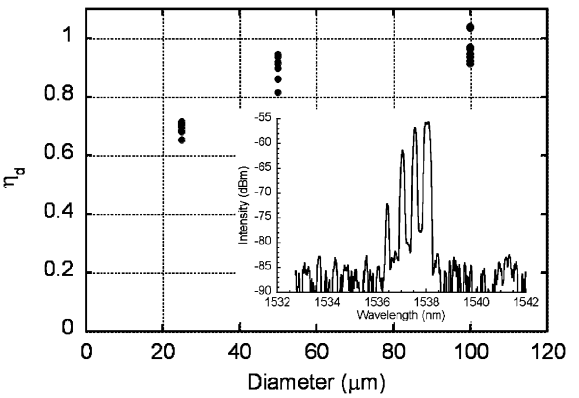

Fig. 8. Light output differential efficiencies for 25, 50, and 100-μm diameter MAR VCSEL devices. The inset shows a spectrum of a 25-μm device biased at 4.5 mA.

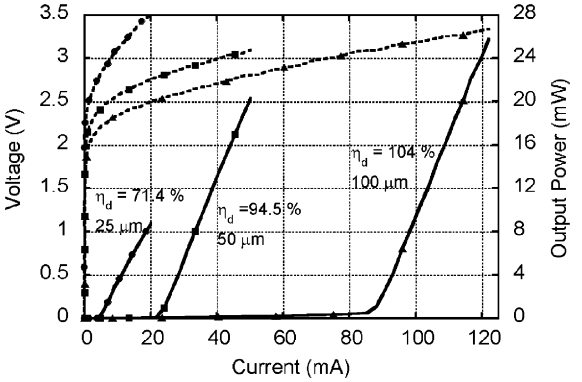

Fig. 9. Light (solid) and voltage (dashed) curves vs. current for a 25-μm (circles), 50-μm (squares), and 100-μm (triangles) diameter device.

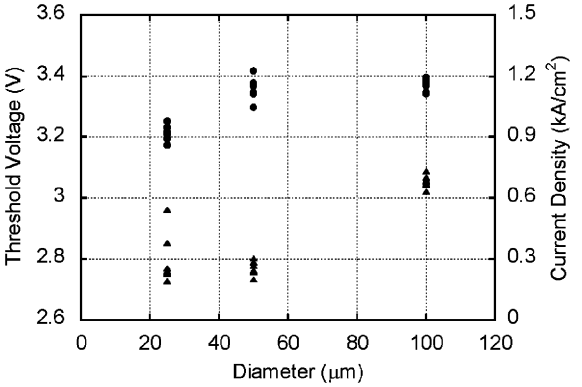

Fig. 10. Threshold voltage (triangles) and threshold current densities (circles) for 25, 50, and 100-μm diameter MAR VCSEL devices.

device is due increased sidewall scattering at smaller device diameters and diffraction loss through bottom DBR. Aperturing the mode would greatly alleviate this scattering and improve towards single mode emission. In addition to the high output efficiency, the devices also exhibited low threshold voltages and threshold current densities, as shown in Fig. 10. For the 25-μm diameter device, threshold voltages were 2.75 V. Subtracting the 2.4 V for the photon energy of a three-stage device, 350 mV remain for the three tunnel junctions and both DBR mirrors. With an estimated 65 mV drop across each tunnel junction measured from a separate investigation, only 155 mV drop across each DBR at a current density of 1 kA/cm^2. This clearly demonstrates both design and growth optimization of each component of the VCSEL to yield low voltage performance. These MAR VCSELs with DAAR, when compared to an identical design using conventional analog-alloy active regions [2], demonstrate comparable performance in terms of output differential efficiency and better performance in terms of voltage and threshold currents. Furthermore, 3-stage MAR edge-emitting lasers with DAAR, fabricated to evaluate active region parameters, performed similarly to previously published MAR edge-emitting lasers with analog-alloy active regions [5]. 3-stage MAR edge-emitting lasers with DAAR exhibited injection efficiencies, η_i, of ~275% and optical losses, α_i, of ~28 cm^{-1}, while those grown with analog-alloy active regions had $\eta_i = 233\%$ and $\alpha_i = 38\,\mathrm{cm}^{-1}$ [5]. This shows that high-quality DAAR with excellent performance can be applied to use in MAR laser structures.

4. Summary

In summary, we have developed high-quality InAlGaAs digital-alloy active regions grown using submonolayer superlattices. These active regions are comparable to their analog counterparts in terms of FWHM. These DAAR were implemented in a 3-stage MAR VCSEL design. The devices exhibited high output differential efficiencies, indicating the good quality and applicability of these DAAR. Greater than 100% output differential quantum efficiencies were achieved along with low voltage and threshold characteristics. Further improvements can be made by including InP, which can be used in the future for ease of aperturing and towards high temperature continuous wave operation.

Acknowledgements

The authors with to thank DARPA for supporting this work via CHIPS. We also want to thank the excellent laboratory support of John English. This work made use of MRL Central Facilities

supported by the MRSEC Program of the National Science Foundation under award No. DMR00-80034.

References

[1] T. Knödl, M. Golling, A. Straub, R. Jäger, R. Michalzik, K.J. Ebeling, IEEE J. Sel. Topics Quantum Electron. 9 (2003) 1406.
[2] J.K. Kim, S. Nakagawa, E. Hall, L.A. Coldren, Appl. Phys. Lett. 75 (2000) 1083.
[3] F. Rana, R.J. Ram, Appl. Phys. Lett. 76 (2000) 1083.
[4] F. Dross, F. van Dijk, B. Vinter., IEEE J. Quantum Electron. 40 (2004) 1003.
[5] J.K. Kim, E. Hall, O. Sjölund, L.A. Coldren, Appl. Phys. Lett. 74 (1999) 3251.
[6] J.G. Cody, D.L. Mathine, R. Droopad, G.N. Maracas, R. Rajesh, R.W. Carpenter, J. Vac. Sci. Technol. B 12 (1994) 1075.
[7] M. Sundaram, A. Wixforth, R.S. Geels, A.C. Gossard, J.H. English, J. Vac. Sci. Technol. B 9 (1991) 1524.
[8] W. Geißelbrecht, U. Pfeiffer, A. Thränhardt, U. Klütz, A.C. Gossard, G.H. Döhler, J. Crystal Growth 201/202 (1999) 163.
[9] M.G. Peters, B.J. Thibeault, D.B. Young, J.W. Scott, F.H. Peters, A.C. Gossard, L.A. Coldren, Appl. Phys. Lett. 63 (1993) 3411.
[10] N. Ohnoki, G. Okazaki, F. Koyama, K. Iga, Electron. Lett. 35 (1999) 51.
[11] S. Jourba, M. Gendry, O. Marty, M. Pitaval, G. Hollinger, Appl. Phys. Lett. 75 (1999) 220.
[12] A.J. Springthorpe, T. Garanzotis, P. Paddon, G. Pakulski, K.I. White, Electron. Lett. 36 (2000) 1031.
[13] G.T. Liu, A. Stintz, E.A. Pease, T.C. Newell, K.J. Malloy, L.F. Lester, IEEE Photon. Tech. Lett. 12 (2000) 4.
[14] M.H.M. Reddy, A. Huntington, D. Buell, R. Koda, E. Hall, L.A. Coldren, Appl. Phys. Lett. 80 (2002) 3509.
[15] M.H.M. Reddy, D.A. Buell, D. Feezell, T. Asano, R. Koda, A.S. Huntington, L.A. Coldren, IEEE Photon. Tech. Lett. 15 (2003) 891.
[16] A.S. Huntington, C.S. Wang, X.G. Zheng, J.C. Campbell, L.A. Coldren, J. Crystal Growth 267 (2004) 458.
[17] A.G. Norman, S.P. Ahrenkiel, H. Moutinho, M.M. Al-Jassim, A. Mascarenhas, J. Mirecki Millunchick, S.R. Lee, R.D. Twesten, D.M. Follstaedt, J.L. Reno, E.D. Jones, Appl. Phys. Lett. 73 (1998) 1844.
[18] J.D. Song, J.M. Kim, J.S. Yu, S.J. Bae, Y.T. Lee, Proceedings of the International Conference on Indium Phosphide and Related Materials, 2002, p. 335.
[19] H. Shimizu, N. Iwai, T. Mukaihara, K. Nishikata, A. Kasukawa, Proceedings of the International Conference on Indium Phosphide and Related Materials, 1997, p. 141.
[20] R. Kiefer, R. Lösch, H. Walcher, M. Walther, S. Weisser, K. Czotscher, W. Benz, J. Rosenzweig, N. Herres, M. Maier, C. Manz, W. Pletschen, J. Braunstein, G. Weimann, Proceedings of the International Conference on Indium Phosphide and Related Materials, 1998, p. 395.
[21] J.M. Elson, J.P. Rahn, J.M. Bennett, Appl. Opt. 22 (1983) 3207.